Int. J. Electrochem. Sci., 10 **(2015)** 8549 - 8557

International Journal of
ELECTROCHEMICAL
SCIENCE
www.electrochemsci.org

A Study on the Corrosion Behavior in Sea Water of Welds Aluminum Alloy by Shielded Metal Arc Welding, Friction Stir Welding and Gas Tungsten Arc Welding

Mustafa Özgür ÖTEYAKA[1,*], *Hamdi AYRTÜRE*[2]

[1]Eskişehir Osmangazi University, Eskisehir Vocational School, Mechatronic Program, 26100, Eskişehir/Turkey
[2] Eskişehir Osmangazi University, Faculty of Engineering, Department of Metalurgy and Materials, 26100, Eskişehir/Turkey
[*]E-mail: moteyaka@ogu.edu.tr

Received: 11 July 2015 / *Accepted:* 6 August 2015 / *Published:* 26 August 2015

Three types of welds aluminum alloy 6061 were prepared using shielded metal arc welding (SMAW), friction stir welding (FSW) and gas tungsten arc welding (GTAW). In addition for the first time borax powder was used with GTAW in weld region to increase the corrosion resistance of aluminum alloys. The corrosion performances of those welds were evaluated in sea water by polarization and impedance techniques. The results of polarization studies and electrochemical impedance spectrometry revealed that borax powders can be used with GTAW technique to increase the corrosion resistance of aluminum alloys. The corrosion potential was lowest for GTAWB (borax powder doped), followed by FSW, GTAW, base metal (BM) and then SMAW as determined using polarization techniques. The rate of corrosion of FSW was found lower compared to other welds. The electrochemical impedance spectrometry (EIS) carried out at a higher frequency exhibited a semicircular loop for friction stir welds, indicating that its corrosion resistance was better than that of the other alloys studied. At medium frequency, the Warburg resistance observed for gas tungsten arc.

Keywords: Aluminum; Polarization; EIS; Corrosion; Welding.

1. INTRODUCTION

In seawater, aluminum alloys experience extremely localized corrosion as a result of the breakdown of the several-nanometer-thick protective oxide film after attack by Cl^- ions. Pitting corrosion characterized by deep pits formed on the surface is generally observed for aluminum alloys covered with aluminum hydroxide [1]. Aluminum alloy 6061, which contains Mg-Si-Cu alloying

elements, is one of the most extensively used alloys because it has desirable properties such as weldability, machinability and corrosion resistance. Major applications of this alloy include its use in aircraft and aerospace components and in the transportation industry [2; 3]. The corrosion resistance of aluminum alloy welds is determined in part by the type of alloy, the filler alloy and the welding process. For aluminum alloys, gas metal arc welding (GMAW) and gas tungsten arc welding (GTAW) are frequently used in welding processes [4-8]. The friction stir welding (FSW) process developed in 1991 by The Welding Institute has also been employed successfully. The advantages of FSW over arc welding processes include improved mechanical properties and reduced microstructural change[9-11]. Few studies have been published on the corrosion and welding of aluminum alloy 6061 [12-15]. According to Nikseresht et al., Fe-rich coarse intermetallic particles act as a cathodic region during the corrosion of 6061 alloy weldment in 3.5 wt. % NaCl. In addition, the weld metal (Ecorr=-704 mV vs. SCE) had better corrosion resistance than the base metal (Ecorr=-728 mV vs. SCE)[6]. In another study, Fahimpour et al. demonstrated that 6061 joined by FSW had higher corrosion resistance than GTAW in seawater solution. However, they reported that both welded regions were susceptible to corrosion attack [4]. Paglia and Buchheit found that aluminum alloy 6061 welded by FSW was susceptible to localized corrosion correlated with precipitate-free zones and coarse precipitates, such as Mg (Zn_2, AlCu). As noted, the localized corrosion began with pitting and propagated as intergranular corrosion [16]. Recently, the hybrid weld technique Nd:YAG laser-GMA was tested on 6061; the result was a more extensive precipitate phase in the weld fusion zone, which resulted in increased pitting corrosion [17].

The study reported herein has been performed to reveal the differences in the corrosion behaviors of 6061 aluminum sheet joined by shielded metal arc welding (SMAW), gas tungsten arc welding (GTAW) and friction stir welding (FSW). In addition, the effect of the addition of borax pentahydrate powder on the corrosion of 6061 joined by GTAW was evaluated for the first time. The free corrosion potential (E_{corr}) was recorded as a function of time. The pitting/repassivation potentials were determined using potentiodynamic curves, cyclic polarization curves and constant-amplitude sinusoidal micropolarization curves, and the resistance of the alloys was measured by impedance techniques.

2. MATERIALS AND METHODS

2.1. Materials and preparations

The materials used were 6061 aluminum alloy sheets with a thickness of 11 mm. Two 30 cm × 20 cm plates were joined together by shielded metal arc welding (SMAW) (electrode EL-AlSi5), gas tungsten arc welding (ER4043 wire) and friction stir welding (FSW). For FSW, a pin rotational speed of 850 rpm and a travel speed of 290 mm/min were used. The $Na_2B_4O_7.5H_2O$-borax pentahydrate powders purchased from Etimaden A.Ş. was used during the GTAW of 6061 aluminum alloy. For simplicity, the base metal, the shielded metal arc welding, friction stir welding, gas tungsten arc

welding and gas tungsten arc welding with borax powder doping are abbreviated as 6061-BM, 6061-SMAW, 6061-FSW, 6061-GTAW and 6061-GTAWB, respectively.

2.3 Corrosion tests

A three-electrode configuration was employed for the electrochemical measurements, featuring a working electrode, a saturated calomel reference electrode (SCE) and a platinum wire counter electrode. The working electrode (1 cm^2) was ground with 800-grit grinding paper, polished with 1-µm diamond paste and stored in 3.5 wt. % NaCl solution for 5 min before each experiment. A Gamry model PC4/300 mA potentiostat/galvanostat controlled by DC105 and EIS300 Corrosion Analysis software was employed in the electrochemical measurements. The free corrosion potential alteration was measured for 6 h. For the potentiodynamic polarization analysis, the potential was scanned from -2000 mV to 750 mV (vs. SCE) at a 1 mV/s scanning rate. The E_{corr}, i_{corr}, βa, βc and corrosion rate were extracted from polarization curves using Gamry software. The new method, constant-amplitude sinusoidal micropolarization (CASP) test was performed at an amplitude (V_a) of 0.5 mV, frequency of 0.1 mHz and potential range of -2400 mV to 1000 mV. Cyclic voltammetry (CV) experiments were conducted at scan rate of 1 mV/s, vertex potential of 1 mV and reverse scan vertex potential of -1 mV. An electrochemical impedance spectrometry (EIS) test was also performed at ±1 V in the frequency range of 50 kHz-0.01 Hz. The EIS spectrum analyzer software converted the EIS results into the equivalent circuit diagram. To assess the reproducibility of the electrochemical tests, each corrosion experiment was repeated three times.

3. RESULTS AND DISCUSSION

3.1 E_{ocp} vs. time measurment

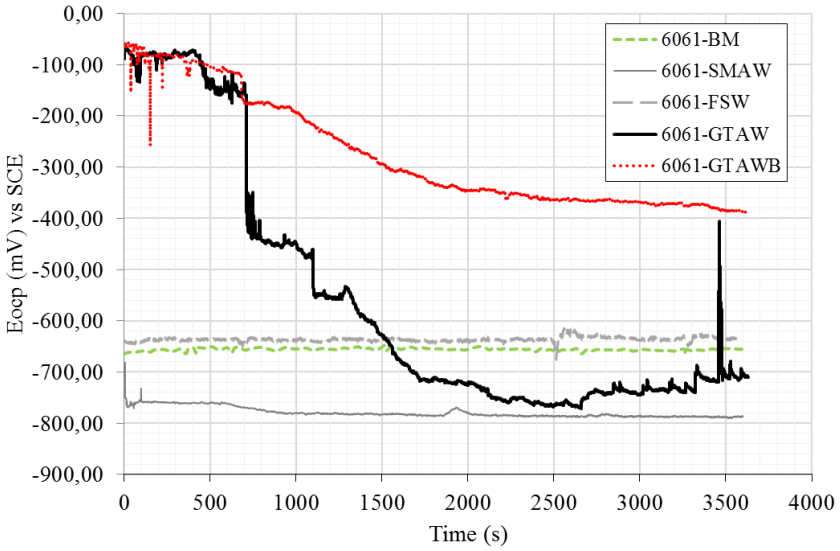

Figure 1. Evaluation of E_{ocp} vs. time for 6061 aluminum alloy base metal and welds in 3.5 wt. % NaCl.

Figure 1 shows the open circuit potential $E_{(ocp)}$ evolution of the 6061 alloy base metal and welds over time in 3.5 wt. % NaCl. The corrosion potential of the base metal at the beginning of the experiment was -670 mV and remained stable throughout the experiment. This potential was comparable with that obtained for 6061-T6 in natural seawater [18]. It should also be noted that upon immersion in a saline environment or contact with water, the aluminum will produce hydrate oxides, such as bayerite ($Al_2O_3.3H_2O$), which functions as a protective layer approximately 2-4 nm in thickness [19]. The FSW sample was slightly more noble than BM, with a corrosion potential of approximately -650 mV at the end of experiment. The GTAW sample exhibited better corrosion resistance than the BM, SMAW, and FSW samples at the beginning of the experiment, especially in the first 10 min. However, the potential then rapidly decreased, and the final corrosion potential recorded was -700 mV, intermediate to the potentials of BM and SMAW. The fluctuation of the potential was observed over the whole surface, indicating the destruction and reformation of the protective oxide film. This phenomenon can be attributed to the intergranular corrosion or passivation and depassivation of pits frequently observed for aluminum alloys [19]. The deeper examination of the corroded samples presented later in this work clarifies the type of corrosion. The corrosion potential of GTAWB was similar to that of GTAW at the beginning of the experiment but then decreased rapidly because of the attack of Cl^- ions on the oxide film. However, the corrosion potential remained stable after 10 min, and no fluctuation was observed over the entire surface of the sample until the end of the experiment. The addition of borax pentahydrate powder during GTAW welding in the joint area made the corrosion potential more noble than that of the other welds tested. The oxide components of boron most likely served as a corrosion barrier, which merits further examination. The final corrosion potential registered for GTAWB was -400 mV, which is the noblest potential observed for any alloy. The most reactive E_{corr} in saline solution was observed for the SMAW sample, being -750 mV at the beginning of the experiment and -790 mV at the end. Peaks observed at 33 min and 50 min suggested susceptibility to localized corrosion.

3.2 Polarization test

Figure 2 shows the polarization curves of the 6061 alloy base metal and welds in 3.5 wt. % NaCl.

Table 1. Results of Tafel polarization studies of the base metal and welds of 6061 aluminum alloys in 3.5 wt. % NaCl.

Welds	Ecorr (mV) vs. SCE	icorr ($\mu A.cm^{-2}$)	βa (mV)	βc (mV)	Corrosion rate (mpy)
6061-BM	-731	3.82	326	371	1.8
6061-SMAW	-781	7.41	191	250	3.6
6061-FSW	-656	4.52	272	397	0.3
6061-GTAW	-698	4.73	336	253	2.2
6061-GTAWB	-429	3.60	268	349	1.7

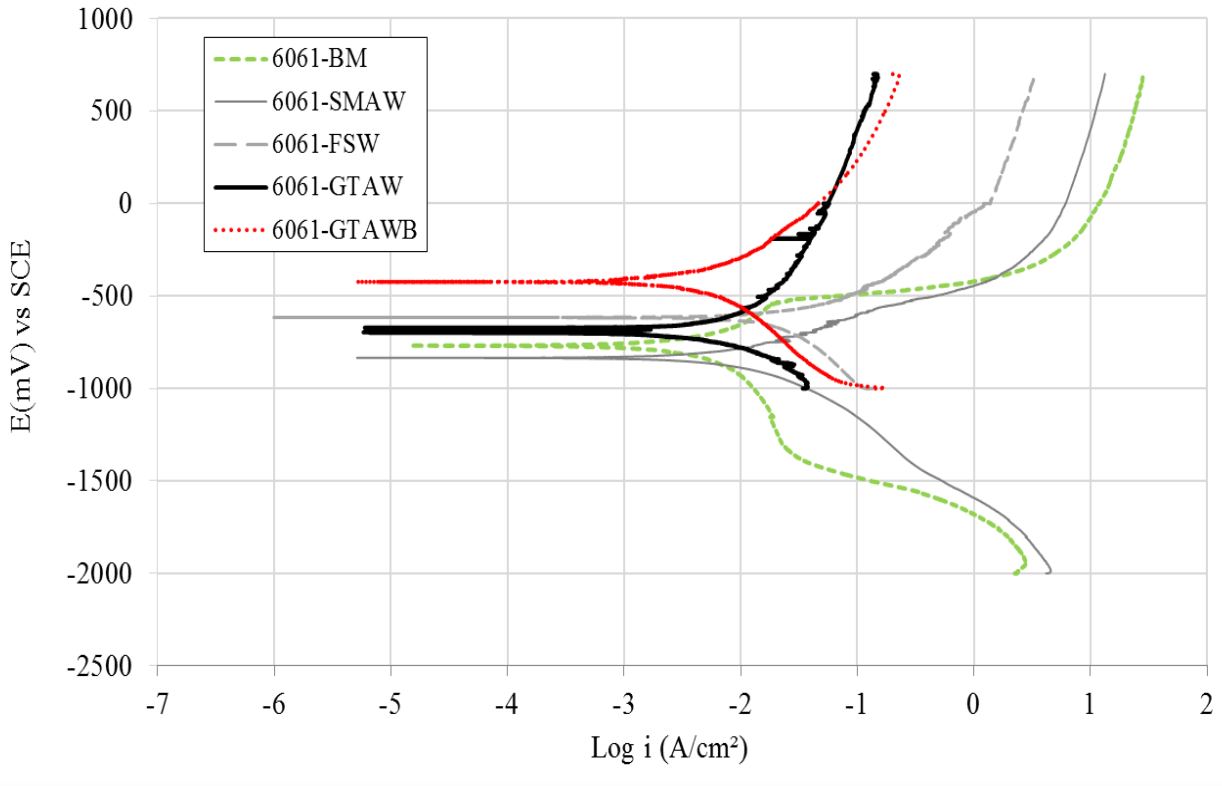

Figure 2. Polarization curves of aluminum alloy 6061 base metal and welds in 3.5 wt. % NaCl (scan rate 1 mV/s).

As observed in figure 2, only the BM, SMAW and FSW samples exhibit passivation behavior. This passivation potential indicates both the beginning of the pitting corrosion potential ($E_{pit.}$) region and the corrosion product's passivation of the pits [19; 20]. The E_{pit} values for BM, SMAW and FSW were -482 mV, -513 mV and -461 mV, respectively. For GTAW and GTAWB, no passivation area was observed in the anodic region, which likely means that pitting occurs in the absence of a protective film.

Table 1 summarizes the E_{corr}, i_{corr}, βa, βc and corrosion rate data extracted from the Tafel curves in figure 2. GTAWB exhibited the best corrosion resistance, with E_{corr} equal to -429 mV and i_{corr} equal to 3.60 ($\mu A.cm^{-2}$), which indicates less dissolution of oxygen (table 1). Meanwhile, SMAW was characterized by the highest corrosion current (7.41 $\mu A.cm^{-2}$) followed by GTAW, FSW and then BM. Although some studies have reported better corrosion resistance for FSW and GTAW than BM, several studies have observed the opposite behavior [4; 21]. The polarization curves obtained are consistent with the observations cited above, namely, that GTAWB had better corrosion resistance than the other welds during the free corrosion potential measurements. In addition to this, the corrosion rate was calculated for each welds; lower corrosion rate was found for FSW (0.3 mpy) while the worst corrosion rate was observed for SMAW (3.6 mpy).

3.3 CASP and CV results

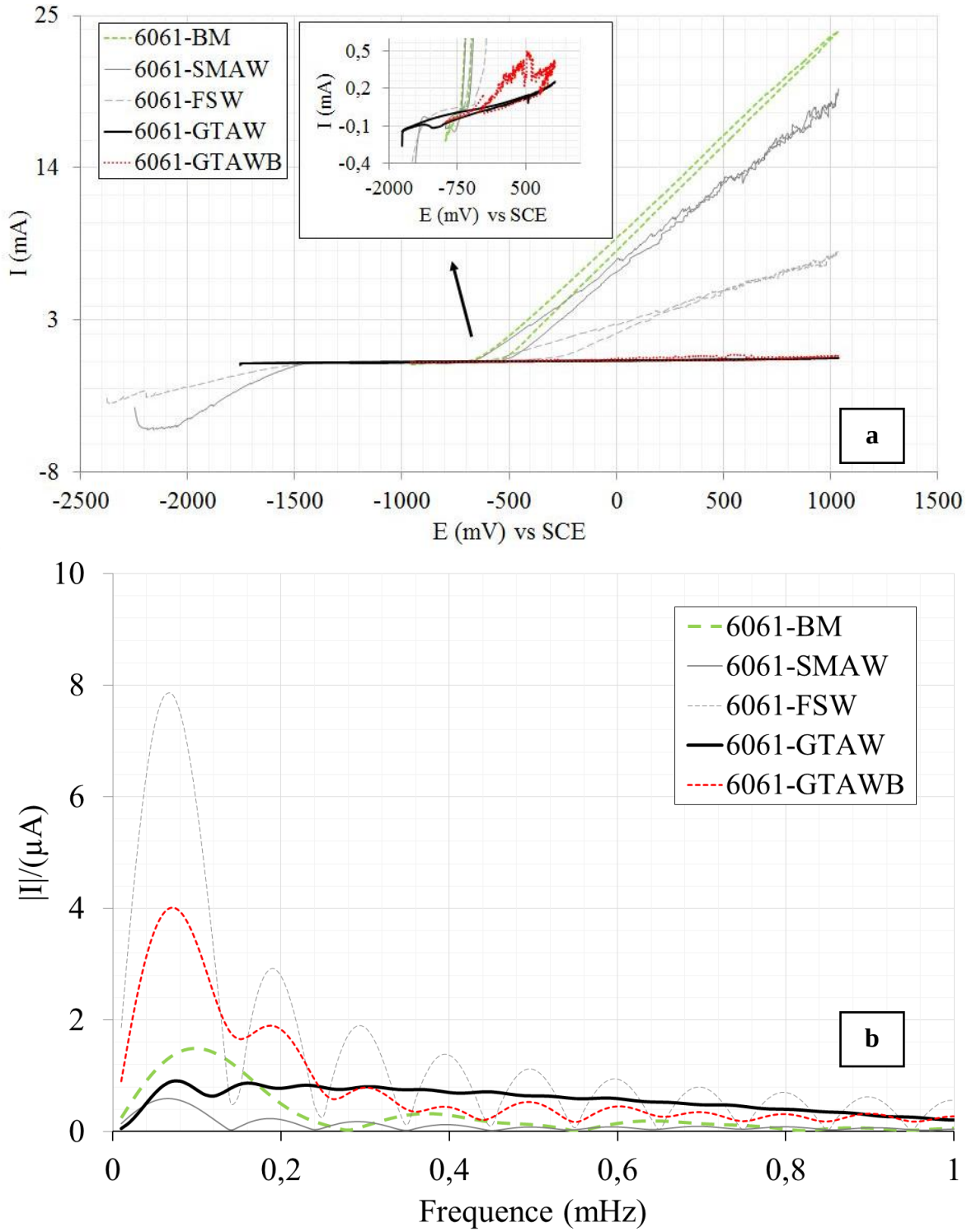

Figure 3. a) Discrete Fourier transform of the current response and b) cyclic voltammogram of the welds.

As described by Gimenze et al. [22], the aluminum alloys in saline environment were susceptible to general attack and pitting corrosion. Constant-amplitude sinusoidal micropolarization (CASP) is a recently developed method for the determination of corrosion parameters, such as

corrosion current, and Tafel parameters during uniform corrosion. In this method, the corrosion current of the samples is measured to compare the uniform and localized corrosion in marine environments. The corrosion current (i_{corr}) was calculated from figure 3a, yielding the following results: BM (0.51 µA), SMAW (0.44 µA), FSW (0.15 µA), GTAW (0.19 µA) and GTAWB (0.16 µA). The welds of FSW, GTAW and GTAWB exhibited better uniform corrosion resistance than BM and SMAW. Cyclic voltammetry (CV) was conducted on the samples, and the findings are shown in figure 3b. BM has the highest anodic current, followed by SMAW, FSW GTAWB and then GTAW. Although a previous study found that aluminum-silicon filler metal had higher corrosion resistance than the base metal, the results above show that SMAW had a lower corrosion resistance than BM [22]. An intense peak was observed prior to the breakdown potential at approximately 500 mV in the chloride solution, which is probably due to the influence of borax. This peak was not observed for the base metal or welds under the same conditions.

3.4 EIS results

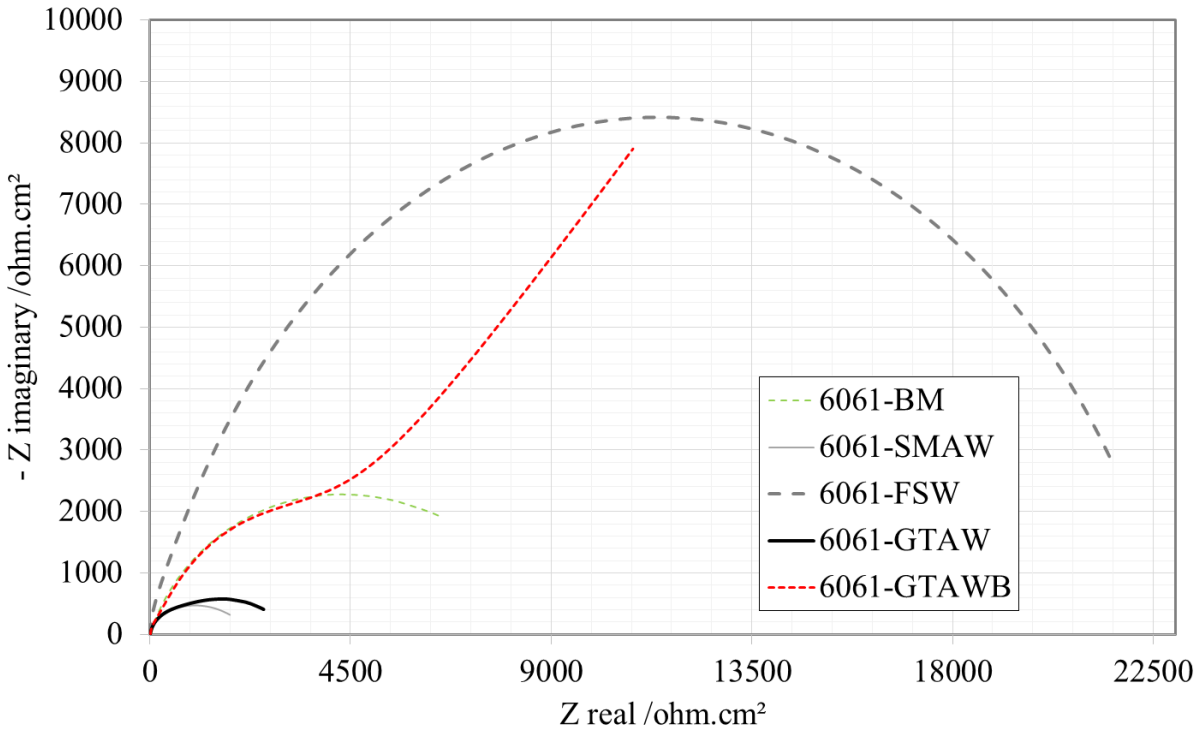

Figure 4. Nyquist plots of the base alloy and welds in 3.5 wt.% NaCl solution.

EIS was used to analyze the uniform and localized corrosion of the base metal and weldments. The EIS method was not suitable for detecting pitting regions because of the difficulty in interpreting the results. However, this method is particularly useful for characterizing the parameters influencing the uniform corrosion rates. Nyquist plots of the samples are shown in figure 4. The curves presented in this figure were simulated using the EIS spectrum analyzer. The Nyquist plots consist of a semicircle, double semicircle and Warburg impedance, as observed in figure 4. Semicircular loops were observed for BM, SWAW, and FSW, while a double semicircle was noticed for GTAW. This

result shows that a single electrochemical reaction is occurring between the solution and the metal surface. FSW had the highest impedance resistance and thus the best corrosion resistance in the saline solution. As illustrated in figure 4., GTAWB exhibits Warburg impedance, corresponding to a diffusion process that limits the mass transfer in the solution and decreases the rate of electrochemical reaction due to blockage of the electrode surface by reaction products or adsorbed solution components.

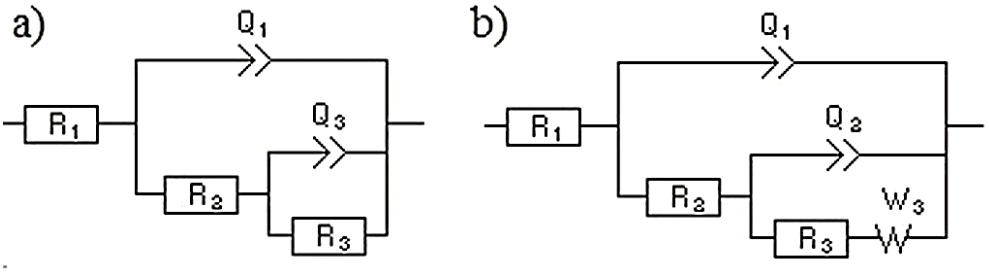

Figure 5. Equivalent circuit model for the corrosion of the base and welds: a) base alloy, AW, SW, and GTAW and b) GTAWB.

As observed in figure 4, two equivalent circuit models can be employed for this system, which are dissimilar to one another due to the complex reaction between the borax powder and solution. The equivalent circuits, shown in figure 5a and 5b, were modeled from the impedance data in figure 4 (data points). In these circuits, R_1, R_2, R_3 and Q are the solution, film, high-frequency capacitive loop and charge transfer resistances, respectively. The passive region (oxide layer aluminum) is associated with R_2, while the corroded region R_3 can be attributed to oxide layer breakdown. Q_1 and Q_2 are constant phase elements corresponding to the high- and middle-frequency capacitive loops, respectively. The constant phase elements are employed in the circuit to refer to the electrode porosity, roughness and inhomogeneity in the samples. The model found for BM conformed to the results reported by Zhang et al [17]. Finally, W_3 is the Warburg impedance, which indicates strong diffusion of ionic species at the interface. Comparing the results of the two models, it is obvious that the borax powder enhanced the corrosion resistance of the weld.

4. CONCLUSIONS

This research demonstrated the corrosion behavior of 6061 welds obtained by shielded metal arc welding (SMAW), friction stir welding (FSW), gas tungsten arc welding (GTAW) and gas tungsten arc welding with borax powder doping (GTAWB). The following conclusions can be drawn:

- Overall, the corrosion resistance in 3.5 wt. % NaCl solution was highest for GTAWB doped with borax powder and lowest for the SMAW weld. An understanding of the role of the borax in the protective film requires a deeper analysis.
- The noblest corrosion potentials recorded during polarization were -429 mV, -656 mV, -698 mV, -731 mV and -781 mV for GTAWB, FSW, GTAW, BM and SWAM, respectively. A passivation zone was observed for FSW, BM and SWAM, which was associated with pitting initiation.

- Localized corrosion, particularly pitting and intergranular corrosion, dominate the welds. The lowest pit propagation in the 3.5 wt. % NaCl solution was found for GTAWB.
- Diffusion resistance at the interface of the GTAWB weld increased its corrosion resistance. In contrast, a single reaction was observed for BM, SWAW, FSW and GTAW. The FSW welds had a higher low-frequency loop than BM, SWAM and GTAW.

ACKNOWLEDGEMENT
The author is grateful to Prof.Dr.Mustafa ANIK (Eskisehir Osmangazi University-Department of Metallurgy and Materials) to help for his comments on the results of electrochemical impedance spectrometry.

Reference

1. R.W. Revie, *Uhlig's Corrosion Handbook*, Wiley, 2011.
2. T. Dursun, C. Soutis, *Materials & Design*, 56 (2014) 862-871.
3. J. Hirsch, *Materials Transactions*, 52 (2011) 818-824.
4. V. Fahimpour, S.K. Sadrnezhaad, F. Karimzadeh, *Materials & Design*, 39 (2012) 329-333.
5. K. Mutombo, M.d. Toit, *International Journal of Fatigue*, 33 (2011) 1539-1547.
6. Z. Nikseresht, F. Karimzadeh, M.A. Golozar, M. Heidarbeigy, *Materials & Design*, 31 (2010) 2643-2648.
7. R. Sathish, V.S. Rao, *Int. J. Electrochem. Sci.*, 9 (2014) 4104-4113.
8. C. Yang, W. Guo, H. Zhang, R. Qiu, J. Hou, Y. Fu, *Int. J. Electrochem. Sci.*, 8 (2013) 9308 - 9316.
9. R. Fu, H. Xu, G. Luan, C. Dong, F. Zhang, G. Li, *Materials Characterization*, 65 (2012) 48-54.
10. A. Simar, Y. Bréchet, B. de Meester, A. Denquin, C. Gallais, T. Pardoen, *Progress in Materials Science*, 57 (2012) 95-183.
11. A. Squillace, A. De Fenzo, G. Giorleo, F. Bellucci, *Journal of Materials Processing Technology*, 152 (2004) 97-105.
12. W.J. Liang, P.A. Rometsch, L.F. Cao, N. Birbilis, *Corrosion Science*, 76 (2013) 119-128.
13. P. Dong, D. Sun, B. Wang, Y. Zhang, H. Li, *Materials & Design*, 54 (2014) 760-765.
14. H.N. McMurray, A. Holder, G. Williams, G.M. Scamans, A.J. Coleman, *Electrochimica Acta*, 55 (2010) 7843-7852.
15. P.M.G.P. Moreira, T. Santos, S.M.O. Tavares, V. Richter-Trummer, P. Vilaça, P.M.S.T. de Castro, *Materials & Design*, 30 (2009) 180-187.
16. C.S. Paglia, R.G. Buchheit, *Scripta Materialia*, 58 (2008) 383-387.
17. D.-Q. Zhang, J. Li, H.G. Joo, K.Y. Lee, *Corrosion Science*, 51 (2009) 1399-1404.
18. S.-j. Kim, S.-j. Lee, J.-y. Jeong, K.-h. Kim, *Transactions of Nonferrous Metals Society of China*, 22, Supplement 3 (2012) s881-s886.
19. E. Ghali, R.W. Revie, *Corrosion Resistance of Aluminum and Magnesium Alloys: Understanding, Performance, and Testing*, Wiley, 2010.
20. M. Oteyaka, E. Ghali, R. Tremblay, *International Journal of Corrosion*, 2012 (2012) 10.
21. W. Xu, J. Liu, H. Zhu, *Electrochimica Acta*, 55 (2010) 2918-2923.
22. P. Gimenez, J.J. Rameau, M.C. Reboul, *Corrosion*, 37 (1981) 673-682.